1.5 GHz TM020-Type Damping Cavity for Ultrafast Transient Experimental Facility

Authors: LI, Dr. Zhongquan, Ye, Dr. Kuangkuang, Dr. Zi-Yang Xu, Dr. Yuanli Luo, Dr. Zhejia Xu, Dr. Lei Yang, Yang, Dr. Yao, Dr. Junqiang Zhang, Dr. Lingxi Ye, Zhou, Xirui, Yang, Ms. Xue, Wang, Mr. Yue, Jie Feng, Hao, Dr. XueRui, Jiang, Dr. Bocheng, Hao, Dr. XueRui

Date: 2025-11-30T00:00:00+00:00

Abstract

This paper presents the comprehensive design, multi-physics analysis of a 1.5 GHz TM020-type damping cavity, engineered for the harmonic RF system of a high-current, low-energy storage ring. While the TM020 mode exhibits inherent advantages for transient beam loading and compact higher-order mode (HOM) damping, its performance is highly sensitive to electromagnetic field leakage caused by perturbations at the field nodes of the fundamental mode. To address this challenge, a systematic design strategy was adopted. The electromagnetic optimization focused on achieving a high intrinsic quality factor and effective HOM damping, incorporating a symmetrically designed triple-tuner assembly to minimize field asymmetry. The input coupler and HOM damping slots were meticulously optimized to balance coupling efficiency, damping capability, and minimization of fundamental mode perturbation. Subsequent multi-physics simulations, including thermal-structural and thermo-mechanical analyses, confirmed the design' s robustness under high-power operation and vacuum conditions, with manageable temperature rise, stress levels, and frequency detuning. The results conclusively confirm the reliability of the proposed TM020-type damping cavity design, establishing a viable path for its application in suppressing coupled-bunch instabilities in modern storage rings.

Full Text

1.5 GHz TM020-Type Damping Cavity for Ultrafast Transient Experimental Facility

Zhongquan Li[1], Kuangkuang Ye[2], Ziyang Xu[2], Yuanli Luo[1], Zhejia Xu[2], Lei Yang[1], Yao Yang[1], Junqiang Zhang[1], Lingxi Ye[1], Xirui Zhou[2], Xue Yang[2], Yue Wang[2], Jie Feng[2], Xuerui Hao[3], ,*, Bocheng Jiang[1],*

[1]Physics Department, Chongqing University
[2]Laboratory for Ultrafast Transient Facility, Chongqing University
[3]Institute of High Energy Physics, 19B Yuquan Road, Beijing 100049, P.R. China
Spallation Neutron Source Science Center, Dongguan, Guangdong 523803, P.R. China

∗Corresponding authors: Xuerui Hao (xrhao@ihep.ac.cn), Bocheng Jiang

Abstract

This paper presents the comprehensive design and multi-physics analysis of a 1.5 GHz TM020-type damping cavity engineered for the harmonic RF system of a high-current, low-energy storage ring. While the TM020 mode exhibits inherent advantages for transient beam loading and compact higher-order mode (HOM) damping, its performance is highly sensitive to electromagnetic field leakage caused by perturbations at the field nodes of the fundamental mode. To address this challenge, a systematic design strategy was adopted. Electromagnetic optimization focused on achieving a high intrinsic quality factor and effective HOM damping, incorporating a symmetrically designed triple-tuner assembly to minimize field asymmetry. The input coupler and HOM damping slots were meticulously optimized to balance coupling efficiency, damping capability, and minimization of fundamental mode perturbation. Subsequent multi-physics simulations, including thermal-structural and thermo-mechanical analyses, confirmed the design' s robustness under high-power operation and vacuum conditions, with manageable temperature rise, stress levels, and frequency detuning. The results conclusively confirm the reliability of the proposed TM020-type damping cavity design, establishing a viable path for its application in suppressing coupled-bunch instabilities in modern storage rings.

Keywords: TM020 mode, electromagnetic field leakage, higher-order modes, magnetic field wave node

1. Introduction

Radiofrequency (RF) cavities serve as critical components in modern accelerator systems, including synchrotron radiation facilities, colliders, and neutron sources, where they fulfill essential functions of particle acceleration, beam bunching, and energy compensation [**?**, **?**, **?**]. The development of fourth-generation synchrotron light sources has exacerbated the issue of coupled-bunch instabilities (CBI), which are primarily attributed to high impedance interactions between charged particle beams and higher-order modes (HOMs) in RF cavities. This pressing issue necessitates the development of

compact HOM-damping cavities with enhanced mode suppression capabilities for next-generation storage rings.

In recent years, the TM020-type damping cavity has emerged as a promising novel RF cavity configuration, attracting considerable attention owing to its inherent unique advantages. The SPring-8 facility and KEK Laboratory have proposed 500 MHz [**?**, **?**] and 1.5 GHz TM020-type damping cavities [**?**], respectively, preliminarily validating the viability of this cavity design. Distinguished from the traditional TM010 mode damping cavity [**?**, **?**, **?**, **?**], the TM020 mode cavity utilizes its unique electromagnetic (EM) field distribution to facilitate a compact HOM absorber structure [**?**]. Moreover, when employed as a harmonic cavity, the TM020-type damping cavity exhibits a reduced R/Q ratio, which effectively mitigates transient effects [**?**]. Notably, despite this lower R/Q, the TM020 mode can achieve a high intrinsic quality factor (Q), thereby maintaining acceptable surface power loss, as governed by $P_c = V_c^2/[(R/Q) \cdot Q_0]$.

The TM020-type damping cavity is designed to strategically place HOM absorbers at the wave nodes of the radial magnetic field or radial electric field. This enables comprehensive absorption of low-order modes (LOMs) and HOMs without compromising the accelerating mode. In 2017, the KEK group first demonstrated a symmetric arrangement of four compact coaxial structures positioned at the radial electric field nodes to simultaneously extract LOMs and HOMs, as reported at the International Particle Accelerator Conference (IPAC' 17) [**?**]. By IPAC' 21, this approach had evolved significantly: researchers proposed a revised methodology that employs a single enlarged coaxial structure aligned with a radial magnetic field node [**?**]. Comparative analyses identified distinct advantages in the magnetic field nodal configuration, particularly in terms of structural simplicity (fewer components) and improved operational stability. These advantages have since facilitated its adoption at major accelerator facilities, including KEK and SPring-8. This paper also focuses on this technical route for research.

Further research on the TM020-type damping cavity reveals several issues that can degrade its RF performance, among which the most critical is EM field leakage of the fundamental accelerating mode. As discussed in previous studies [**?**, **?**], such leakage is highly sensitive to the position of HOM coupling slots with respect to the magnetic field nodes of the operating mode. Even minor deviations near these nodal points—where the radial magnetic field exhibits a steep gradient—can result in significant field leakage caused by local breakdown of the ideal field boundary conditions. Moreover, any disruption of the azimuthal symmetry of the EM field distribution, typically induced by asymmetrically positioned auxiliary components such as input couplers or tuners, can further exacerbate energy leakage from the accelerating mode.

The primary factors contributing to the disruption of EM field distribution symmetry include the input coupler and the tuner structure. Such effects can be minimized through the symmetrical arrangement of tuners [**?**]. The impact of the input coupler, which feeds power into the RF cavity and interacts strongly

with it, is particularly notable for its influence on the symmetry of the field distribution. To address the issue of EM field leakage from the operating mode of the TM020-type damping cavity, the ESRF-EBS project team has proposed implementing choke structure as a secondary measure to protect the TM020 mode. Accordingly, the team has designed a set of 1.409 GHz TM020-type 2-cell room-temperature damping cavities, as detailed in [**?**]. Incorporating choke structure effectively protects the TM020 mode against severe EM field leakage arising from positional offsets of coupling slots and displacement of wave nodes. However, this approach impedes the transmission of other deleterious modes, which in turn diminishes the damping effect.

Table 1: UTEF storage ring machine parameters

Parameter	Value
Beam energy	0.5 GeV
Beam current	0.5–1.0 A
Damping time (, ,)	59/59/29.5 ms
Damping time with feedback (,)	0.05/0.05 ms
Momentum compaction factor	0.16
Working point (,)	8.15
Main RF frequency	499.784 MHz
Third harmonic frequency	1.499352 GHz
Bunch length	2.7 mm
Bunch length after bunch lengthening	12.2 mm

This paper presents the comprehensive design of a 1.5 GHz TM020-type damping cavity for the dual-RF system of the 0.5 GeV storage ring at the Ultrafast Transient Experimental Facility (UTEF), whose key parameters are listed in Table 1 [**?**, **?**]. Our work focuses on a holistic optimization strategy that moves beyond merely protecting the TM020 mode. We systematically address the interconnected challenges of HOM damping, power coupling, frequency tuning, and multipacting suppression. The design incorporates a symmetric triple-tuner configuration to minimize field asymmetry and employs refined damping slot geometries to balance fundamental mode confinement with effective HOM absorption. The final cavity design achieves robust performance across all critical metrics, including RF efficiency, beam stability, and thermo-mechanical reliability, providing a viable solution for high-current, long-bunch applications.

2. RF Design

The overall design of an RF cavity is an iterative process involving cavity optimization, absorber design, coupler design, tuner design, multipacting analysis, and multiphysics simulation. The design process begins with EM optimization

of the cavity geometry to meet the target resonant frequency, shunt impedance, and quality factor. Subsequent steps involve designing and optimizing the absorber, coupler, and tuner. The absorber design must achieve a balance between protecting the accelerating mode and effectively suppressing HOMs. The coupler design should meet the required fundamental coupling coefficient while introducing minimal perturbation to the EM field distribution of the operating mode, thereby avoiding significant field leakage. The tuner design must provide an adequate frequency tuning range and avoid inducing substantial EM field leakage. The final step involves conducting a multipacting analysis to ensure that the damping cavity operates without multipacting under the designated operating conditions.

A schematic of the vacuum assembly for the TM020-type damping cavity is shown in [FIGURE:1], depicting the complete cavity structure along with its components: the absorber, coupler, tuner, signal extractor, and vacuum pump port. The corresponding structural parameters are labeled, which serves as the reference configuration for all subsequent optimization studies.

2.1. Feasibility Analysis of the TM020 Mode as an Accelerating Mode

This section demonstrates the feasibility and unique advantages of employing the TM020 mode as an accelerating mode, based on the analytical framework for a cylindrical pillbox cavity. For a pillbox cavity of radius R and length L, the resonant frequency for a TM_{mnp} mode is given by the equation:

$$f_{mnp} = \frac{c}{2\pi}\sqrt{\left(\frac{x_{mn}}{R}\right)^2 + \left(\frac{p\pi}{L}\right)^2}$$

where c is the speed of light in a vacuum, and x_{mn} is the n-th root of the derivative of the m-th-order Bessel function $J'_m(x) = 0$. For the family of TM_{0n0} modes with no axial dependence ($p = 0$), this equation simplifies to:

$$f_{0n0} = \frac{c \cdot x_{0n}}{2\pi R}$$

[FIGURE:2] shows the magnetic field distribution diagrams for different resonant modes in a pillbox cavity. A fundamental attribute of the TM020 mode, akin to that of the conventional TM010 mode, is the presence of an axially uniform and non-zero longitudinal electric field E_z along the cavity axis. This field profile is indispensable for the efficient acceleration of charged particles, thereby establishing the theoretical viability of employing the TM020 mode in accelerator applications.

To quantitatively compare the cavity geometries, the cavity radii required for a resonant frequency of 1.5 GHz are calculated. With the roots $x_{01} \approx 2.405$ corresponding to the TM010 mode and $x_{02} \approx 5.520$ corresponding to the TM020 mode, the respective radii are:

- **TM010:** $R_{010} = \frac{c \cdot x_{01}}{2\pi f} \approx 76.6$ mm
- **TM020:** $R_{020} = \frac{c \cdot x_{02}}{2\pi f} \approx 175.7$ mm

The larger dimensions of the TM020-type cavity confer several key operational advantages over its TM010 counterpart. For a fixed axial length, the TM020 geometry provides a substantially greater surface area and internal volume, which enhance heat dissipation from RF losses, thereby mitigating thermal management issues, enabling higher power-handling capacities, and improving pressure tolerance. Additionally, the TM020 mode features a lower R/Q, defined as $(V_c)^2/(2\omega U)$ where V_c is the accelerating voltage, ω the angular frequency, and U the stored energy; this reduced R/Q diminishes the induced voltage from beam-current perturbations, thereby suppressing transient beam-loading effects and bolstering accelerator stability. Furthermore, the azimuthal magnetic field H_ϕ of the TM020 mode vanishes precisely at the radial position of its second magnetic node—unlike most HOMs, which exhibit significant field strengths there; this nodal property facilitates the placement of damping absorbers at that location to selectively attenuate unwanted HOMs with negligible perturbation to the fundamental mode, while promoting a more compact cavity design.

2.2. RF Design of the Proof of Principle Cavity

This section presents a detailed study on the main cavity (Proof-of-Principle, POP, as shown in [FIGURE:1]a) of the TM020-type damping structure, focusing on the optimization and analysis of the TM020 mode' s RF parameters (R/Q and Q_0) and the cavity' s HOMs and lower-order modes (LOMs).

2.2.1. Accelerating Mode The geometry of the POP cavity was optimized to operate in the TM020 mode at a target frequency of 1499.352 MHz. We performed a parametric scan of key dimensions—including the cavity length (L), curvature radii (C_3, R_0), and iris properties (l_0)—to maximize the intrinsic quality factor (Q_0) while minimizing the R/Q. As shown in [FIGURE:3], this optimization successfully yielded a cavity geometry with a high Q_0 and a low R/Q, exhibiting performance aligned with the objectives of alleviating transient beam-loading effects and enhancing power handling efficiency. The final optimized parameters are listed in .

Table 2: RF parameters of the accelerating mode for POP cavity

Parameter	Value
Eigenmode freq.	1499.352 MHz
R/Q	56.6 Ω
Q_0	3.62×10^4
R_a	2.04 MΩ

2.2.2. Wake and Impedance The interaction of electron bunches with the accelerating cavity can excite wakefields that encompass both LOMs and HOMs.

These EM resonances pose a significant risk, as they can cause emittance growth and energy spread, and ultimately induce coupled-bunch instabilities (CBI). To ensure beam stability, it is imperative to control the cavity' s HOM impedance to ensure it stays below the critical CBI threshold. The CBI threshold for such systems can be determined using well-established analytical formulas [**?**]:

$$Z_{th}^{\parallel} = \frac{2 \cdot (E_0/e) \cdot Q_s}{I_b \cdot \alpha_p \cdot \tau_s}$$

$$Z_{th}^{\perp} = \frac{2 \cdot (E_0/e)}{f_{rev} \cdot I_b \cdot \beta_{x,y} \cdot \tau_{x,y}} L$$

where $Z_{th}^{\parallel}$ and $Z_{th}^{\perp}$ are the total longitudinal and transverse impedance thresholds, respectively; $f_{\parallel,HOM}$ is the longitudinal HOM frequency, E_0 is the beam energy, e is the electron charge, I_b is the average beam current, Q_s is the synchrotron tune, α_p is the momentum compaction factor, f_{rev} is the revolution frequency, $\tau_{x,y,s}$ are the damping times and $\beta_{x,y}$ are the beta functions at the cavity location. The longitudinal and transverse impedance thresholds are subsequently calculated using Eq. 1 2, with parameters as listed in .

Notably, the implementation of a dual-frequency RF system (fundamental + third harmonic) increases the longitudinal impedance threshold, while a feedback system improves the transverse impedance threshold [**?**]. [FIGURE:4] presents the distribution of longitudinal and transverse impedances for the resonant modes of the POP cavity, which compares these impedances to their respective thresholds. The results demonstrate that several undamped HOMs exceed the stability limits, highlighting the need to incorporate an effective HOM damping structure.

2.3. HOM Coupling Slot Design

This section details the design and optimization of the HOM coupling slot for the damping cavity. The design strategy is based on the EM field distribution of the fundamental TM020 mode. As shown in

, the azimuthal magnetic field H_ϕ of the TM020 mode exhibits two radial null points (nodes). Positioning the coupling slot at these nodes allows for the integration of HOM dampers while theoretically preserving the integrity of the fundamental mode, as its magnetic field—and thus its stored energy—is subject to minimal perturbation at these locations.

However, the region near the field node is characterized by a high spatial gradient of the magnetic field. A first-order approximation for the magnetic field near the nodal point r_0 is given by:

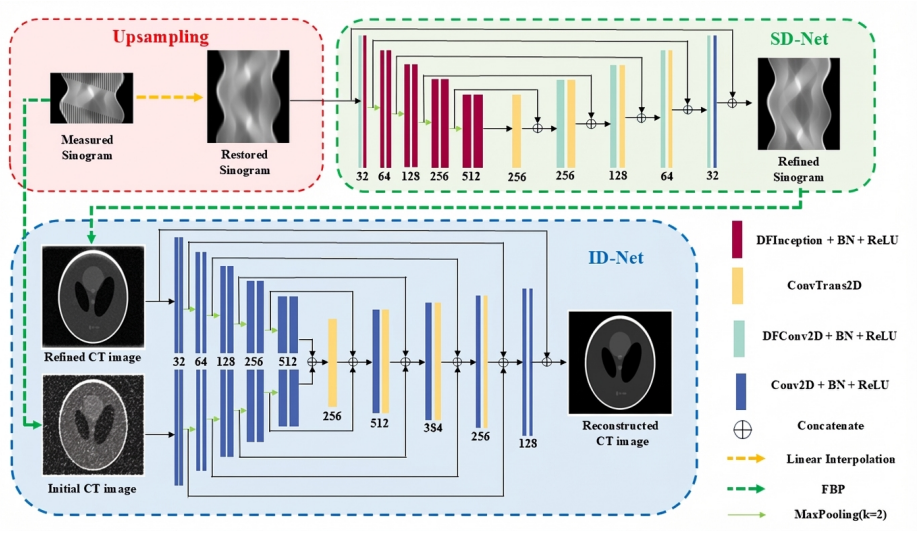

Figure 1: Figure 5

$$H_\phi(r) \approx \left.\frac{dH_\phi}{dr}\right|_{r=r_0} \Delta r$$

where Δr is a small displacement from the node. This linear relationship indicates that even a minor positional offset Δr of the slot from the ideal node r_0 results in a non-zero magnetic field coupling, which in turn leads to significant EM field leakage and degradation of the fundamental mode' s quality factor (Q_0). Consequently, the primary challenge in design is to optimize the slot' s geometry and position to desensitize the structure to manufacturing tolerances and minimize this leakage.

The proposed slot design, illustrated in [FIGURE:1]b, incorporates a 90-degree bent configuration with the absorber positioned at the corner. The initial optimization centered on the slot widths: the straight section width (d_h) and the bent section width (H_x). The initial study, with d_h and H_x set equal, investigated the effect of slot width on field leakage sensitivity. The results, summarized in [FIGURE:6]a, demonstrate that wider slots increase the sensitivity of fundamental mode leakage to positional misalignment.

Subsequently, with d_h held constant, the parameter H_x was adjusted over a range of values. The analysis (as shown in [FIGURE:6]b) demonstrates that increasing H_x also exacerbates the positional sensitivity. This trend is attributed to a reduction in the slot' s transmission efficiency ($\eta[\%] = (1 - |S_{11}|^2) \times 100$) across a broad frequency range, as confirmed by the frequency-domain analysis in [FIGURE:7]a. A lower η hinders the effective extraction and damping of

HOM energy.

A conflicting design requirement emerged from the analysis of a specific harmful mode, TM021, shown in [FIGURE:7]b. Specifically, increasing H_x leads to a higher shunt impedance of the TM021 mode, which is detrimental as it strengthens the beam-cavity interaction for this unwanted mode. Therefore, effective damping of HOMs such as TM021 requires a smaller H_x, while desensitizing the fundamental mode to slot misalignment requires a larger H_x.

After a comprehensive trade-off study, an optimal configuration was identified with $H_x = 10$ mm and $d_h = 8$ mm. This set of parameters successfully balances the competing objectives: it sustains sufficiently high transmission efficiency to enable effective HOM damping, while achieving an acceptable degree of insensitivity to potential slot positioning deviations, thus ensuring the robust operational performance of the fundamental TM020 mode.

2.4. Coupler Design

This section presents the design of the high-power input coupler, a critical component tasked with efficiently delivering microwave power from the source to the RF cavity. However, the introduction of a coupler, necessitating strong coupling, inherently perturbs the EM field distribution of the fundamental TM020 mode. This perturbation can be understood through the lens of EM boundary conditions: the insertion of the coupler' s metallic conductors distorts the original field pattern, resulting in a radial shift Δr_n in the position of the magnetic field nodes. Consequently, a non-zero magnetic field arises at the target nodal location, which compromises the effectiveness of HOM dampers installed at these positions and causes undesirable field leakage. The strength of the leakage field is proportional to the product of the local field gradient and the nodal shift, i.e., $E_{leak} \propto |\nabla H_\phi| \cdot \Delta r_n$.

Therefore, the coupler design must achieve dual-objective optimization: meeting the target coupling coefficient β while minimizing the induced nodal shift and the resulting fundamental mode field leakage. The proposed coupler geometry is illustrated in [FIGURE:1]b. A parametric study was conducted to navigate this design trade-off, with the key findings as follows:

- **Outer Conductor Radius ($R_{coupler}$):** The radius of the coupler' s outer conductor exerts a significant influence on both objectives. As shown in [FIGURE:8]a, an increase in $R_{coupler}$ leads to a simultaneous increase in both the coupling coefficient β and the field leakage rate. This is attributed to a larger physical intrusion into the cavity volume, which causes more substantial perturbation to the field distribution.
- **Inner Conductor Penetration Depth ($L_{tp.coupler}$):** The penetration depth of the inner conductor primarily governs the coupling strength. [FIGURE:8]b demonstrates that reducing $L_{tp.coupler}$ effectively decreases the coupling coefficient β with only a marginal effect on field leakage.

This parameter acts as the primary tuning tool for achieving the target β without severely exacerbating leakage.

- **Choke Depth (*chkp*):** The depth of the capacitive choke (*chkp*) is a key feature for suppressing field leakage. As quantified in [FIGURE:8]c, increasing *chkp* enhances the impedance seen by stray fields, thereby effectively reducing the field leakage rate. A larger *chkp* also slightly lowers the coupling coefficient due to the increased distance between the inner conductor tip and the cavity volume. While a larger *chkp* benefits leakage suppression, a minimum value of 10 mm is imposed by mechanical and high-voltage standoff requirements for the coupler assembly.
- **Inner Conductor Rotation (*Rot.coupler*):** The rotational orientation of the inner conductor offers an additional degree of freedom for fine-tuning coupling. As evidenced in [FIGURE:8]d, varying the rotation angle θ enables fine control of the coupling coefficient β with negligible impact on field leakage. This parameter is typically used as a final adjustment to meet specific coupling requirements without compromising the cavity' s field confinement.

In summary, the coupler design requires a systematic trade-off between competing objectives. The final geometry was determined by first setting *chkp* to its minimum feasible value to minimize leakage; then adjusting $R_{coupler}$ to reach the target coupling regime; and finally utilizing $L_{tp.coupler}$ and θ to precisely tune β. This methodology ensures robust power coupling while effectively mitigating the detrimental perturbation to the cavity' s fundamental mode.

2.5. Tuner Design

This section describes the design of the frequency tuner, a crucial subsystem designed to fine-tune the resonant frequency of the fundamental TM020 mode, compensate for manufacturing tolerances and detuning effects during operation, and thereby ensure optimal cavity performance. Similar to the input coupler, the introduction of a tuner structure into the cavity volume perturbs the EM boundary conditions. This perturbation locally deforms the EM field distribution, causing a shift in the magnetic field nodes of the TM020 mode and resulting in EM field leakage. The primary design challenge, therefore, is to achieve a sufficient tuning range while maintaining acceptably low field leakage.

To mitigate the disruptive impact on the field distribution, a symmetric configuration with three identical tuners was adopted, as illustrated in [FIGURE:1]b. The symmetric arrangement is intended to cancel out the dominant dipolar-component field perturbations, thereby preserving the azimuthal symmetry of the TM020 mode and minimizing the net levels of field distortion and leakage.

The core tuning mechanism relies on the insertion of a tuner pin (inner conductor) into the cavity. The fundamental frequency shift can be qualitatively understood through the Slater perturbation theorem [**?**, **?**]. The theorem states

that the resonant frequency shift Δf is related to the change in the cavity' s stored EM energy. Inserting a metallic tuner pin into a region of predominantly electric field lowers the resonant frequency, while inserting it into a magnetic field region raises it. In this design, the tuner is positioned to interact with the fringe fields, where a deeper insertion (increasing the penetration depth parameter $L_{tp.tuner}$) effectively increases the capacitive loading, thereby reducing the resonant frequency.

[FIGURE:9]b plots the resonant frequency and normalized field leakage rate as functions of the tuner penetration depth $L_{tp.tuner}$. The results align with theoretical expectations: the resonant frequency decreases monotonically with increasing $L_{tp.tuner}$. A tuning range from 1500.99 MHz to 1498.45 MHz is achieved over the mechanical travel range of $L_{tp.tuner}$ from -10 mm to 10 mm, successfully covering the target frequency of 1.499352 GHz.

Concurrently, the field leakage rate displays non-monotonic behavior, with a distinct minimum observed within the scanning range. This minimum corresponds to the tuner position that optimally compensates for the field perturbation introduced by its own structure. Crucially, over the practical operational range of $L_{tp.tuner}$ from -8 mm to 10 mm, the field leakage rate remains below the 2% threshold, indicating that effective frequency tuning can be accomplished without compromising the EM integrity of the accelerating mode.

In summary, the symmetric three-tuner design provides the necessary frequency adjustment capability while effectively controlling levels of field leakage, ensuring stable and efficient operation of the TM020-type cavity.

2.6. TM020-Type Damping Cavity Analysis

Following the successful design of the HOM damper, high-power input coupler, and tuner for the Proof-of-Principle (POP) cavity, this section presents the integrated cavity analysis with the addition of the signal extraction port and vacuum pumping structure. The comprehensive EM characterization encompasses the fundamental accelerating mode, as well as beam-cavity interaction effects induced by wakefields and impedance.

2.6.1. Accelerating Mode The key structural parameters of the final integrated cavity design are summarized in . The corresponding EM field distribution of the fundamental TM020 accelerating mode is depicted in [FIGURE:10], confirming the desired field pattern and the proper integration of all ancillary components. The critical RF parameters that quantify the accelerating efficiency and power dissipation of the TM020 mode—namely the intrinsic quality factor (Q_0), the characteristic impedance (R/Q), and the shunt impedance (R_a) —are listed in . These values are consistent with the design objectives outlined in previous sections.

Table 3: Key structural parameters of the TM020-type damping cavity

Parameter	Value (mm)
d_h	8
L_h	82
R_t	175.7
$R_{coupler}$	30
R_{tuner}	10

Table 4: RF parameters of the accelerating mode for the TM020-type damping cavity

Parameter	Value
freq.	1499.539 MHz
R/Q	56.6 Ω
Q_0	3.62×10^4
R_a	2.05 MΩ

2.6.2. Wake and Impedance Analysis To assess beam stability, a rigorous analysis of wakefields and beam-coupling impedance was conducted. The longitudinal wake potential $W_z(\tau)$ left by a leading charged particle induces an energy loss on trailing particles, potentially leading to beam instability. This effect is characterized by the beam-coupling impedance; for a specific mode, this impedance is given by:

$$Z = \frac{1}{2}(R/Q) \cdot Q_L$$

where Q_L is the loaded quality factor of the mode, determined by the damping structures. A higher impedance indicates a stronger interaction between the beam and the cavity mode.

The initial identification of potentially dangerous HOMs was performed via the eigenmode solver in CST Microwave Studio [**?**], analyzing all modes below the beam-pipe cut-off frequency. The identified HOMs and LOMs, along with their simulated R/Q and Q_L values, are cataloged in .

Table 5: Analysis of RF parameters for HOMs and LOMs

Mode	freq. (MHz)	R/Q (Ω)	Z_L (kΩ)	Mode	freq. (MHz)	R/Q (Ω/m)	Z_T (kΩ/m)
TM021	2378.5	12.3	1.85	TM120	1895.2	45.6	2.34
TM121	2456.8	8.7	1.42	TE111	1987.3	32.1	1.89

Subsequently, a direct wakefield computation was performed using the transient solver of CST Particle Studio. A Gaussian bunch with a charge of 2 nC and a length (σ_z) of 12.2 mm was tracked through the cavity structure, and the wake potential was computed over a length of 200 m. The resulting wakefield is shown in [FIGURE:12]. The beam-coupling impedance for each mode was evaluated and compared against the established instability threshold for the accelerator' s beam parameters.

The analysis reveals that one mode, the TM021, has an impedance that exceeds the safety threshold. Two other modes, TM120 and TM121, lie close to the threshold and are classified as critical. The magnetic field distributions of these three potentially harmful modes are illustrated in [FIGURE:11], providing insight into their spatial structure and interaction with the damping slots. All other HOMs were found to have impedances far below the threshold, confirming that the overall damping design is effective and meets the required design specifications.

2.7. Multipacting Analysis

Multipacting is a resonant phenomenon in RF structures wherein free electrons, driven by oscillating EM fields, follow trajectories leading to repeated impacts on the structure' s surfaces. An electron avalanche occurs when the impact energy and the surface' s secondary electron yield (SEY) collectively result in a net gain of electrons per impact cycle. The condition for multipacting is quantified by the secondary emission yield [**?**]:

$$\langle SEY \rangle = \frac{n_{emission}}{n_{collision}} = \frac{I_{emission}}{I_{collision}}$$

where $n_{collision}$ and $n_{emission}$ are the numbers of primary incident and secondary emitted electrons, respectively, with $I_{collision}$ and $I_{emission}$ being the corresponding currents. Multipacting initiates when $SEY > 1$, which leads to exponential growth in the electron population over successive generations m, as described by:

$$N_{e,m} = N_0 \langle SEY \rangle^m$$

which is equivalent to the temporal growth $\log N(t) = \log N_0 + \alpha t$ with a positive growth factor α.

To evaluate multipacting risks in the 1.5 GHz TM020-type damping cavity, a series of simulations were performed using CST Particle Studio. The analysis focused on high-risk regions, including the loop-type input coupler, the inner wall of the HOM coupling slot, the cavity side wall, and the nose cone, as illustrated in [FIGURE:13]a. Primary electron sources were set up with a kinetic energy of 2 eV, an energy spread of 20%, and an angular spread of 85° to comprehensively sample initial conditions. The copper-ECSS probabilistic secondary

emission model was employed, which tracks up to 50 electron generations with a maximum of 2.5 secondaries per hit. The SEY characteristics of the surface material, highly dependent on processing technology, are shown in [FIGURE:13]b, comparing the copper-ECSS and copper-Furman models.

The simulations scanned accelerating voltages from 0.05 MV to 0.5 MV and RF phases from 0° to 360° in steps of 45°. The results, summarized in [FIGURE:13], demonstrate that across the designated operational voltage range of 0.1 MV to 0.45 MV, the effective SEY remains consistently below unity under all phase conditions. This confirms that the cavity design, coupled with the selected surface treatment, successfully suppresses multipacting, ensuring stable high-power operation.

---

3. Mechanical and Thermal Analysis

A mechanical design for the high-power cavity model has been developed, with its 3D CAD assembly illustrated in

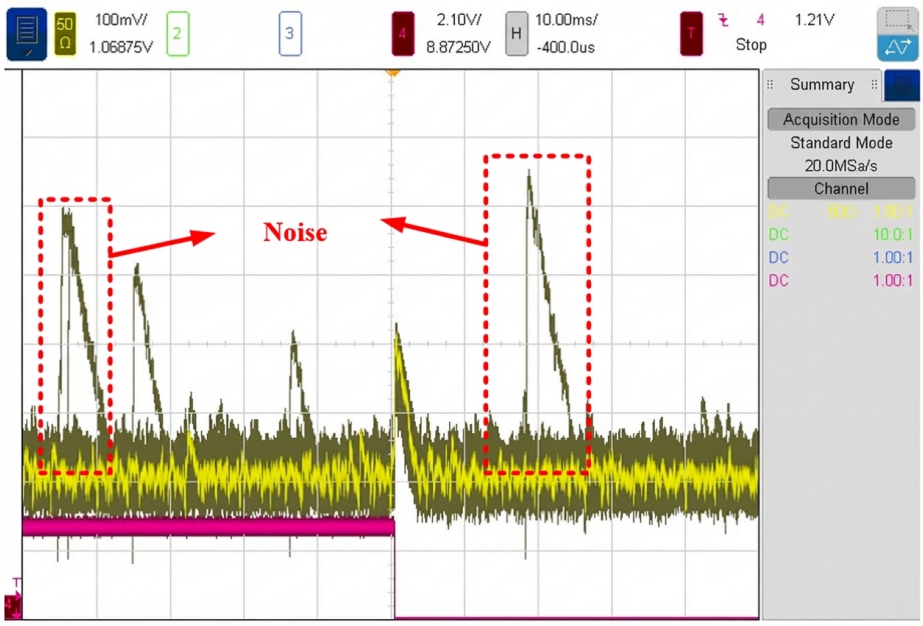

Figure 2: Figure 14

. The cavity assembly consists of a main cavity body, two endplate assemblies, and twelve absorber modules.

The main cavity body is fabricated from oxygen-free high-conductivity (OFHC) copper, with stainless steel flanges brazed onto it. Each endplate assembly

features an OFHC copper inner wall and nose cone, which are also brazed onto a stainless steel backing plate. A stainless steel bridge plate, featuring six openings for the absorber modules, serves to structurally support the endplate assembly and is brazed to it, forming a complete unit. Each absorber module comprises six ferrite tiles, a copper base, and a stainless steel flange. The ferrite tiles are brazed onto the copper base, which is integrated with internal cooling water channels. Vacuum sealing among the main body, bridge plates, and absorber modules is accomplished via metal O-rings or gaskets.

To account for potential manufacturing tolerances, the critical structural parameter 'Gap' was adjusted from its nominal design value of 82 mm to 81.6 mm in the final mechanical design. This parameter can be further optimized during commissioning to fine-tune the resonant frequency to the desired value. The adjusted structural parameters and their corresponding high-frequency parameters for the accelerating mode are summarized in .

Table 6: RF parameters corresponding to the machining scheme

Scheme	Gap (mm)	freq. (MHz)	R/Q (Ω)	Q_0 (10^4)	R_a (MΩ)
opt.	82.0	1499.539	56.6	3.62	2.05
mach.	81.6	1499.352	56.8	3.61	2.06

3.1. Thermal Analysis and Cooling System Design

Thermal management of the TM020-type damping cavity is critical for stable operation. The total thermal load originates from two primary sources: (1) resistive surface losses on the cavity inner walls, which scale with the input RF power, and (2) power dissipated in the HOM dampers, arising from both the fundamental mode leakage and energy from beam-excited HOMs. An effective cooling system is designed to remove this heat. The first step in its analysis is to characterize the flow regime within the cooling channels. The convective heat transfer coefficient (h) is determined using established correlations for internal flow. The hydraulic diameter d is defined as:

$$d = \frac{4S}{L}$$

where S is the flow cross-sectional area and L is the wetted perimeter. The flow regime is identified by the Reynolds number:

$$Re = \frac{\rho v d}{\eta}$$

where ρ is the fluid density, v the flow velocity, and η the dynamic viscosity. A flow velocity between 2 and 3 m/s is maintained as a design trade-off to

effectively remove heat without inducing mechanical vibration [**?**]. For 35°C inlet cooling water in the designed channels, $Re = 40,805$, which confirms the flow is turbulent ($10^4 < Re < 1.2 \times 10^5$).

For turbulent flow in smooth tubes with a length-to-diameter ratio greater than 60, the Dittus-Boelter correlation is valid. The convective heat transfer coefficient is calculated as:

$$h = 0.023 \frac{k_w}{d} Re^{0.8} Pr_w^n$$

Here, k_w is the thermal conductivity of water, Pr_w the Prandtl number, and the exponent n is set to 0.4 for heating (wall to fluid) [**?**, **?**]. Using the aforementioned thermophysical parameters, the calculated value of h is approximately 9,000 W/(m^2 · K), ensuring efficient heat removal from the cavity structure.

3.1.1. Thermal Analysis of the Main Cavity A steady-state thermal analysis of the main cavity was performed to assess its thermal performance under high-power operation. The analysis is governed by the steady-state heat conduction equation with a volumetric heat source:

$$\nabla \cdot (k \nabla T) + \dot{q} = 0$$

where k is the thermal conductivity, T the temperature, and $\dot{q}$ the heat generation rate per unit volume, calculated from the RF surface power losses on the cavity walls. The primary heat source is the resistive dissipation of RF surface currents, which is quantified as the surface power loss. The resulting heat is removed by the forced convective cooling system, with the water-cooling channels modeled using a convective boundary condition.

Three scenarios with different surface power losses—20 kW, 30 kW, and 40 kW—were conducted to evaluate the thermal response. As illustrated in [FIGURE:15], the corresponding surface power density increased proportionally with the total surface power loss. The temperature distribution under the prescribed design cooling conditions, obtained via a CST Multiphysics simulation, is presented in

.

The results confirm a positive correlation between the input power and the cavity' s temperature rise. Crucially, even at the maximum simulated power of 40 kW, the peak temperature rise remains below 43 °C. At a lower power of 20 kW, the maximum temperature rise is less than 22 °C, demonstrating effective heat dissipation. Key parameters, including the maximum temperature rise and the design-required coolant flow rate for each case, are compiled in . These results confirm that the cavity' s cooling design is adequate for managing the anticipated thermal loads and maintains acceptable temperature margins.

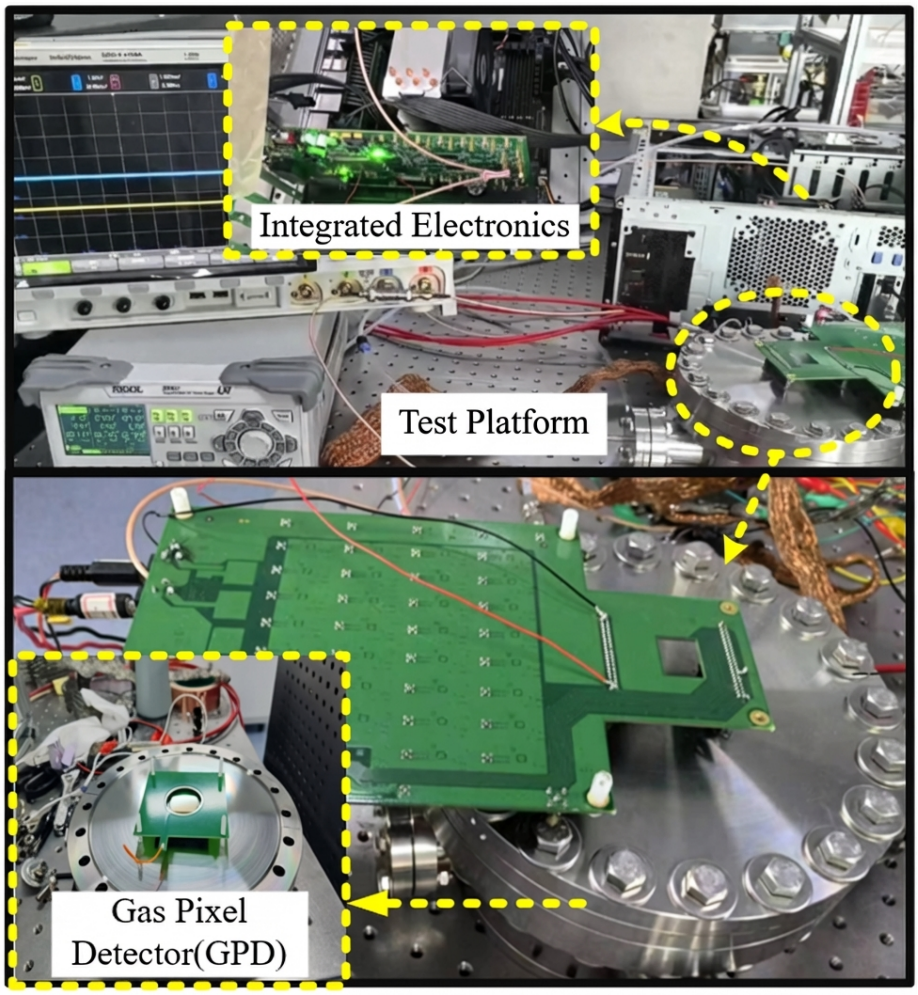

Figure 3: Figure 16

Table 7: Temperature analysis of the cavity and cooling water under different surface power losses

P_c (kW)	ΔT (K)	Flow Rate (L/s)	Max. ΔT (water)	Max. ΔT (cavity)	h (W/(m^2 · K))
20	14.9	0.8	10.2	14.9	10,160
30	21.7	1.2	14.8	21.7	10,160
40	28.5	1.6	19.4	28.5	10,160

3.1.2. Thermal-Structural Analysis of the Ferrite Absorber The thermal load on the absorber modules originates from two primary sources: power dissipation from beam-excited HOMs and leakage from the fundamental TM020 mode. The power from HOMs is rigorously evaluated using the wakefield-based formalism [**?**]. The total longitudinal loss factor k_t is extracted from a CST Particle Studio simulation, from which the HOM-specific loss factor k_{HOM} is derived by subtracting the fundamental mode loss factor k_0, calculated as:

$$k_0 = \frac{\omega_0}{2}\left(\frac{R}{Q}\right)_0$$

Subsequently, the HOM power dissipation is given by $P_{HOM} = k_{HOM} \cdot q \cdot I_0$. With simulated values of $k_0 = 0.13$ V/pC and $k_t = 0.66$ V/pC, the calculated P_{HOM} under nominal beam operation is 1.06 W. This is complemented by power from the fundamental TM020 mode leakage. Assuming a conservative field leakage rate of 2% (equivalent to 800 W for a 40 kW input power), the total estimated power deposited on the absorber modules is below 2 kW. To ensure operational robustness, a worst-case scenario with a total absorbed power of 2 kW was adopted for the subsequent thermal-structural simulation. The mechanical layout of the absorber assembly is shown in [FIGURE:17]a.

A coupled multiphysics simulation was performed, applying this power load with a spatial profile derived from EM simulations. The steady-state temperature distribution is shown in [FIGURE:17]b. The peak temperature of the ferrite tiles was found to be significantly below the Curie temperature of Ni-Zn ferrite (typically >100 °C), thereby ensuring stable EM properties and eliminating the risk of thermal demagnetization.

The corresponding thermo-mechanical stress distribution was analyzed, with the von Mises stress distribution presented in [FIGURE:17]c. The maximum calculated stress at the critical ferrite-copper base interface was approximately 30 MPa. Given that the typical tensile strength of Ni-Zn ferrite ranges from 20 to 50 MPa [**?**], this results in an acceptable safety factor, confirming the structural integrity of the absorber design under the prescribed thermal load. Key material properties and performance metrics are summarized in .

Table 8: Mechanical and thermal properties of ferrite materials

Property	Value	Unit	Reference Standard
Mechanical properties [?]			
Tensile Strength	35	MPa	GB/T 1040.2-2006
Tensile Modulus	120	GPa	GB/T 23805-2009
Flexural Strength	85	MPa	GB/T 6569-2006
Compressive Strength	450	MPa	GB/T 8489-2006
Poisson' s Ratio	0.25	-	GB/T 23805-2009
Thermal performance [?]			
Specific Heat Capacity	0.85	J/(g · °C)	GB/T 3810.3-2016
Density	5.2	g/cm³	Laboratory Method
Coefficient of Thermal Expansion (30-400°C)	10.2	×10 /°C	GB/T 7320-2018
Coefficient of Thermal Expansion (30-800°C)	11.5	×10 /°C	GB/T 7320-2018
Thermal Conductivity (25°C)	5.8	W/(m · K)	GB/T 7320-2018

3.2. Thermo-Mechanical Deformation and Its Impact on RF Performance

The mechanical and thermal analyses presented earlier validate the structural and cooling design of the TM020-type damping cavity. However, the spatially nonuniform thermal expansion, induced by RF power dissipation, generates significant thermal stress within the cavity' s inner walls. Concurrently, the structure is subject to atmospheric pressure loading during vacuum operation. The superposition of these thermo-mechanical loads results in a predictable deformation of the cavity geometry, which in turn disturbs the cavity' s internal EM field distribution, leading to shifts of the resonant frequency and degradations in field confinement.

The fundamental relationship between the temperature field and the resultant deformation is governed by the thermoelastic constitutive equations. The total strain ϵ_{total} is decomposed into the elastic strain and thermal strain:

$$\epsilon_{total} = \epsilon_{elastic} + \alpha(T - T_0)I$$

where α is the coefficient of thermal expansion, T the temperature distribution, T_0 the stress-free reference temperature, and I the identity tensor. The resulting stress field, calculated via Hooke' s law, and the external pressure load together govern the displacement field u.

To quantify this effect, coupled thermal-structural simulations were performed for surface power losses of 20 kW, 30 kW, and 40 kW. The first set of results, shown in [FIGURE:18] (Thermal Stress Distribution), demonstrates that the maximum von Mises stress within the cavity structure increases with the applied RF power. The second set, presented in [FIGURE:19] (Mechanical Deformation), illustrates the corresponding deformation. The magnitude of the cavity' s maximum structural displacement increases from 66.5 µm at 20 kW to 134 µm at 40 kW.

This mechanical deformation directly perturbs the cavity' s EM boundaries. According to Slater' s perturbation theorem, a uniform inward displacement of the cavity' s inner walls typically lowers the resonant frequency. The simulated impact of this deformation on RF performance is summarized in . As the deformation increases with thermal load, the resonant frequency exhibits a negative shift, escalating from -177 kHz at 20 kW to -357 kHz at 40 kW.

Table 9: RF parameters of the accelerating mode for the TM020-type damping cavity under different surface power loss conditions

P_c (kW)	freq. (MHz)	Δf (kHz)	Q_0 (10^4)	Q_m (10^6)
20	1499.362	-177	3.61	13.352
30	1499.342	-197	3.60	21.973
40	1499.322	-357	3.58	29.217

Furthermore, the cavity' s mechanical deformation affects the EM field leakage. This occurs through two mechanisms: first, the geometrical distortion disrupts the precise alignment of the HOM coupler slots relative to the magnetic field nodes; second, a shift in the resonant frequency alters the spatial distribution of the field nodes. Despite these effects, the simulation results reveal that the increase in the EM field leakage rate is negligible. It rises only from 2.09% under a cold, unpowered condition to 2.12% at 20 kW and 2.14% at 40 kW. This minimal change confirms the robustness of the cavity' s structural and HOM damping design against expected thermo-mechanical deformations.

4. Summary

This paper presents the comprehensive design and multi-physics analysis of a 1.5 GHz TM020-type damping cavity for the harmonic RF system of the Ultrafast Transient Experimental Facility storage ring, operating at 0.5 GeV beam energy and 0.5–1.0 A current. The TM020 mode offers advantages in mitigating transient beam loading with a reduced R/Q of 56.6 Ω and high intrinsic quality factor Q_0 of 3.62×10^4, while enabling compact higher-order mode damping. Performance is sensitive to electromagnetic field leakage at fundamental mode field nodes, addressed through a systematic optimization incorporating a symmetric triple-tuner assembly for minimal field asymmetry, optimized input coupler with coupling coefficient $\beta \approx 3.2$, and HOM damping slots with dimensions $H_x = 10$ mm and $d_h = 8$ mm to balance damping efficiency (transmission $\eta > 90\%$ for HOMs) and fundamental mode confinement (leakage $< 1\%$). Multi-physics simulations confirm robustness under 40 kW operation, with maximum temperature rise < 43°C, von Mises stress < 30 MPa in absorbers, and frequency detuning < 357 kHz. The design establishes a reliable solution for suppressing instabilities in high-current storage rings, with bunch lengthening from 2.7 mm to 12.2 mm. Future work will focus on high-power prototyping and beam tests to confirm performance in operational environments.

CRediT Authorship Contribution Statement

Xuerui Hao: Writing - review & editing, Writing - original draft, Validation, Software, Methodology, Investigation, Data curation, Conceptualization.
Bocheng Jiang: Validation, Software, Methodology, Investigation, Data curation, Conceptualization.
Zhongquan Li: Writing - review & editing, Writing - original draft, Supervision, Resources, Project administration, Methodology, Data curation, Conceptualization.
Kuangkuang Ye: Writing - review & editing, Writing - original draft, Software, Methodology, Data curation, Conceptualization.
Ziyang Xu: Writing - review & editing, Writing - original draft, Software, Methodology, Data curation, Conceptualization.
Jie Feng: Resources, Investigation.
Yue Wang: Resources, Investigation.
Yuanli Luo: Resources, Investigation.
Xue Yang: Resources, Investigation.
Lingxi Ye: Resources, Investigation.
Lei Yang: Resources, Investigation.
Yao Yang: Resources, Investigation.
Zhejia Xu: Resources, Investigation.
Junqiang Zhang: Resources, Investigation.
Xirui Zhou: Resources, Investigation.

Acknowledgements

This work is partly supported by Laboratory for Ultrafast Transient Facility (LUTF) project, Chongqing University.

Data Availability

The data supporting the findings of this study are available from the corresponding author upon reasonable request.

References

[1] A. Smygacheva, V. Korchuganov, Y. Fomin, Coupled bunch instabilities in the storage rings, in: XXV Russian Particle Accelerator Conference (RuPAC-2016), 2017, pp. 395–397.
[2] R. R. Lindberg, Theory of coupled-bunch longitudinal instabilities in a storage ring for arbitrary rf potentials, Physical Review Accelerators and Beams 21 (2018) 124402.
[3] P. Tavares, F. Cullinan, Å. Andersson, D. Olsson, R. Svärd, Beam-based characterization of higher-order-mode driven coupled-bunch instabilities in a fourth-generation storage ring, Nuclear Instruments and Methods in Physics Research Section A: Accelerators, Spectrometers, Detectors and Associated Equipment 1021 (2022) 165945.
[4] H. Ego, J. Watanabe, S. Kimura, K. Sato, Design of a hom-damped rf cavity for the spring-8-ii storage ring, in: Proc. the 11th Annual Meeting of Particle Accelerator Society of Japan (PASJ2014), 2014.
[5] H. Ego, H. Tanaka, T. Inagaki, T. Ohshima, H. Yamaguchi, T. Tomai, T. Asaka, N. Nishimori, Compact hom-damping structure of a beam-accelerating tm020 mode rf cavity, Nuclear Instruments and Methods in Physics Research Section A: Accelerators, Spectrometers, Detectors and Associated Equipment 1064 (2024) 169418.
[6] T. Yamaguchi, N. Yamamoto, D. Naito, T. Takahashi, S. Sakanaka, Design and low-power measurement of 1.5 ghz tm020-type harmonic cavity for kek future synchrotron light source, Nuclear Instruments and Methods in Physics Research Section A: Accelerators, Spectrometers, Detectors and Associated Equipment 1053 (2023) 168362.
[7] X. Hao, Z. Li, K. Ye, P. Wang, G. Wei, J. Li, J. Wang, 500 mhz higher order mode damped cavity designed for 4th generation synchrotron radiation sources, Nuclear Instruments and Methods in Physics Research Section A: Accelerators, Spectrometers, Detectors and Associated Equipment 1040 (2022) 167273.
[8] E. Weihreter, F. Marhauser, Hom damped cavities for high brilliance synchrotron light sources, in: Brilliant Light in Life and Material Sciences, Springer, 2007, pp. 413–427.
[9] F. Marhauser, E. Weihreter, D. Dykes, P. McIntosh, Hom damped 500 mhz cavity design for 3rd generation sr sources, Proceedings of the 2001 Particle

Accelerator Conference (Cat. No. 01CH37268), volume 2, IEEE, 2001, pp. 846–848.
[10] R. Rimmer, D. Li, Design considerations for a second generation hom-damped rf cavity, in: Proceedings of the 1999 Particle Accelerator Conference (Cat. No. 99CH36366), volume 2, IEEE, 1999, pp. 907–909.
[11] T. Yamaguchi, S. Sakanaka, N. Yamamoto, D. Naito, T. Takahashi, et al., Optimization of the parasitic-mode damping on the 1.5 ghz tm020-type harmonic cavity, in: 12th International Particle Accelerator Conference (IPAC'21), Campinas, SP, Brazil, 24-28 May 2021, 2021, pp. 1064–1067.
[12] J. Byrd, S. De Santis, J. Jacob, V. Serriere, Transient beam loading effects in harmonic rf systems for light sources, Physical Review Special Topics-Accelerators and Beams 5 (2002) 092001.
[13] T. Takahashi, S. Sakanaka, N. Yamamoto, et al., Design study of damped accelerating cavity based on the tm020-mode and hom couplers for the kek light source project, in: 8th Int. Particle Accelerator Conf.(IPAC' 17), Copenhagen, Denmark, 14–19 May, 2017, JACOW, Geneva, Switzerland, 2017, pp. 4172–4175.
[14] T. Yamaguchi, S. Sakanaka, N. Yamamoto, D. Naito, T. Takahashi, et al., Optimization of the parasitic-mode damping on the 1.5 ghz tm020-type harmonic cavity, in: 12th International Particle Accelerator Conference (IPAC'21), Campinas, SP, Brazil, 24-28 May 2021, JACOW Publishing, Geneva, Switzerland, 2021, pp. 1064–1067.
[15] X. Hao, J. Zhu, X. Li, Z. Liu, C. Zhang, W. Long, S. Chen, Y. Liu, S. Liu, B. Wu, A study of the electromagnetic fields leakage in tm020 mode hom-damped cavity, Nuclear Engineering and Technology 57 (2025) 103717.
[16] Z. Li, K. Ye, L. Yang, Y. Zhang, X. Zhou, X. Yang, X. Hao, Electromagnetic field compensation to attenuate energy leakage in tm020 mode damped cavity, Nuclear Engineering and Technology 57 (2025) 103256.
[17] T. Yamaguchi, N. Yamamoto, D. Naito, T. Takahashi, S. Sakanaka, Design and low-power measurement of 1.5 ghz tm020-type harmonic cavity for kek future synchrotron light source, Nuclear Instruments and Methods in Physics Research Section A: Accelerators, Spectrometers, Detectors and Associated Equipment 1053 (2023) 168362.
[18] A. D'Elia, et al, HarmonLip 2024, 2024. URL: https://indico.esrf.fr/event/122/contributions/668/attachme
[19] Y. Zhang, B. Jiang, Z. Bai, D. Xiang, A high-current low-energy storage ring for photon-hungry applications, in: Proceedings of the 14th International Particle Accelerator Conference, Venice, Italy, 2023, pp. 368–371.
[20] G. Penco, M. Svandrlik, Experimental studies on transient beam loading effects in the presence of a superconducting third harmonic cavity, Physical Review Special Topics—Accelerators and Beams 9 (2006) 044401.
[21] A. W. Chao, Physics of Collective Beam Instabilities in High Energy Accelerators, John Wiley & Sons, New York, 1993.
[22] R. Bosch, Instability analysis of an active higher-harmonic cavity, in: Proceedings of the 1997 Particle Accelerator Conference (Cat. No. 97CH36167), volume 1, IEEE, 1997, pp. 862–864.
[23] H. Padamsee, J. Knobloch, T. Hays, RF Superconductivity for Accelerators,

John Wiley & Sons, 1998.
[24] J. C. Slater, Microwave Electronics, D. Van Nostrand, New York, 1950.
[25] CST Microwave Studio®, Ver. 2020, CST DS SIMULIA, Darmstadt, Germany., www.cst.com, 2020.
[26] T. Khabiboulline, et al., Multipacting in the ilc 1.3 ghz hom coupler, in: Proceedings of the International Particle Accelerator Conference (IPAC 2015), JACoW Publishing, 2015, pp. 1234–1236.
[27] G. Shu, J.-R. Zhang, X.-T. Zhang, H.-W. Yuan, Y.-L. Chi, Multi-physics analysis of a 325 mhz bi-periodic on-axis coupled accelerating structure, Radiation Detection Technology and Methods 1 (2017) 1–5.
[28] W. S. Janna, Engineering heat transfer, CRC press, 2018.
[29] F. Kreith, The CRC handbook of thermal engineering, Springer Science & Business Media, 2000.
[30] G. V. Stupakov, Wake and impedance, in: AIP Conference Proceedings, volume 592, AIP, 2001, pp. 205–230.
[31] Stand Testing, Inspection Report on Mechanical Properties, Test Report STD-20200714-039N, Stand Testing, China, 2020. Laboratory environmental conditions: (21-22) °C, (53-54)% RH. Focus on tensile strength, modulus, flexural strength, compressive strength, and Poisson' s ratio properties.
[32] Stand Testing, Inspection Report on Thermal Properties, Test Report STD-20190903-032N-3, Stand Testing, China, 2019. Test results were derived from parallel data. Focus on specific heat capacity, thermal expansion, and conductivity.
[33] Products guide -soft ferrite-, document number hj-b3-e (pdf), proterial, ltd., 2009. URL: https://www.proterial.com/e/products/elec/tel.